Published in final edited form as:
J Phys Chem C Nanomater Interfaces. 2011 December 15; 115(49): 24247–24255. doi:10.1021/jp208035x.

ToF-SIMS Analysis of Adsorbed Proteins: Principal Component Analysis of the Primary Ion Species Effect on the Protein Fragmentation Patterns

Shin Muramoto[1,3], **Daniel J. Graham**[1,2], **Matthew S. Wagner**[4], **Tae Geol Lee**[5], **Dae Won Moon**[5], and **David G. Castner**[1,3,§]

[1]National ESCA and Surface Analysis Center for Biomedical Problems, University of Washington, Seattle, WA 98195

[2]Department of Bioengineering, University of Washington, Seattle, WA 98195

[3]Department of Chemical Engineering, University of Washington, Seattle, WA 98195

[4]The Procter & Gamble Company, Cincinnati, OH 45202

[5]Center for Nano-Bio Convergence, Korean Research Institute of Standards and Science, Daejeon 305-340, Korea

Abstract

In time-of-flight secondary ion mass spectrometry (ToF-SIMS), the choice of primary ion used for analysis can influence the resulting mass spectrum. This is because different primary ion types can produce different fragmentation pathways. In this study, analysis of single-component protein monolayers were performed using monatomic, tri-atomic, and polyatomic primary ion sources. Eight primary ions (Cs^+, Au^+, Au_3^+, Bi^+, Bi_3^+, Bi_3^{++}, C_{60}^+) were used to examine to the low mass (m/z < 200) fragmentation patterns from five different proteins (bovine serum albumin, bovine serum fibrinogen, bovine immunoglobulin G and chicken egg white lysozyme) adsorbed onto mica surfaces. Principal component analysis (PCA) processing of the ToF-SIMS data showed that variation in peak intensity caused by the primary ions was greater than differences in protein composition. The spectra generated by Cs^+, Au^+ and Bi^+ primary ions were similar, but the spectra generated by monatomic, tri-atomic and polyatomic primary ion ions varied significantly. C_{60} primary ions increased fragmentation of the adsorbed proteins in the m/z < 200 region, resulting in more intense low *m/z* peaks. Thus, comparison of data obtained by one primary ion species with that obtained by another primary ion species should be done with caution. However, for the spectra generated using a given primary ion beam, discrimination between the spectra of different proteins followed similar trends. Therefore, a PCA model of proteins created with a given ion source should only be applied to datasets obtained using the same ion source. The type of information obtained from PCA depended on the peak set used. When only amino acid peaks were used, PCA was able to identify the relationship between proteins by their amino acid composition. When all peaks from *m/z* 12-200 were used, PCA separated proteins based on a ratio of $C_4H_8N^+$ to K^+ peak intensities. This ratio correlated with the thickness of the protein films and Bi_1^+ primary ions produced the most surface sensitive spectra.

[§]Corresponding Author: Dept of Chemical Engineering Box 351750 University of Washington Seattle, WA 98195-1750 1-206-543-8094 castner@nb.uw.edu .

Supporting Information PCA results for ToF-SIMS data from adsorbed Lys and IgG films on mica are provided in the supporting information.

Keywords

bismuth; C60; cluster ion; PCA; thin films

1. Introduction

Time-of-flight secondary ion mass spectrometry (ToF-SIMS) is a powerful surface analysis technique for the characterization of adsorbed protein films due to its high surface sensitivity, molecular specificity, and lateral resolution [1-5], allowing it to identify a particular protein from a multi-component protein film [6, 7]. However, the interpretation of ToF-SIMS data from adsorbed protein films is challenging because large, unique secondary ion fragments from a given protein are typically not detected, unlike matrix-assisted laser desorption/ionization (MALDI), which yields high mass molecular ions from large non-volatile biomolecules [8, 9]. Without large, unique fragments, the complex variations in the low mass (0-200 m/z) ToF-SIMS fragmentation pattern from the 20 amino acids present in proteins must be analyzed to determine an adsorbed protein's identity, concentration, conformation and orientation. For proteins, these small mass fragments are usually fragments of individual amino acids, as significant levels of tripeptides, dipeptides, and even monopeptides are not detected. To decode the information in the low mass fragmentation patterns, investigators have identified characteristic peaks that correspond to each of the 20 amino acids [2]. However, since all proteins contain the same 20 amino acids, ToF-SIMS data from adsorbed proteins cannot be easily differentiated based on the presence or absence of unique peaks. Due to the multivariate nature of the data, methods such as principal component analysis (PCA) become invaluable. PCA can aid in the interpretation of mass spectra by revealing differences between each spectrum (scores), and relating them back to the differences in the fragmentation pattern of the spectra (loadings), the utility of which has been demonstrated by our group [3, 5, 7, 10-16], as well as other groups [17-20]. The combination of using characteristic peaks for a given system with PCA has proven to be an effective methodology in aiding with the interpretation of spectral data. The use of multivariate analysis methods with ToF-SIMS data has increased dramatically in the last decade [21]. These techniques have been used to probe the orientation and conformation of adsorbed proteins [15, 16, 22], as well as to identify and differentiate specific proteins in mixtures [6, 7].

Recent advances in primary ion technology have focused on the development of cluster ion beams. The most important landmark in primary ion advancement has been the increase in secondary ion yield from the development of cluster ion sources such as SF_6^- [23], Au_n^+ (n = 1-5) [24], Bi_n^{q+} (n = 1-7, q = 1 and 2) [25], and C_{60}^{q+} probes (q = 1-3) [26, 27]. Historically, primary ion sources commonly used in SIMS experiments have been monatomic projectiles such as Ar^+, Xe^+, Ga^+ and Cs^+. However, the level of chemical information obtained using these monatomic projectiles was low. This was in part due to the low yield of ionized fragments (< 1%) [28], as well as the inefficient desorption of large fragments that contain greater chemical complexity. Many techniques such as matrix enhancement [29, 30], metal cationization [31-33], and laser-post ionization of neutrals [34] have been employed to increase yields, especially with the goal of emitting large mass fragments. The development of cluster primary ions led to the observation that for some systems one not only gets an increase in overall yield of all secondary ions, but the yield enhancement is more pronounced in the higher mass region (i.e., m/z > 200) of the spectrum [35]. This has been observed across multiple sample types: hard substrates such as metals; bulk polymers which can be considered to have an intermediate hardness; rat brain and bacterial cells which are usually treated as soft bulk materials [18, 25, 36]. However,

detailed examination of mixtures of soft and hard samples such as thin protein films adsorbed onto mica are still needed.

One shortcoming of cluster ion species, which has been extensively examined, is that they seem to cause a change in the fragmentation pattern of the sputtered material when compared to monatomic ion species [18]. This means that when mass spectra of atomic and cluster ion sources are compared for the same sample, there can be differences in the relative intensities of ionized fragments. Although it is known that atomic and cluster ion sources produce different secondary ion yields, which is related to the sputter yield and ionization efficiency of the sputtered material as well as the ion source, the mechanism by which the intensity of certain sputtered fragments are enhanced or reduced remains unclear. Understanding how the various ion sources affect the fragmentation pattern is of significant importance since changes in the fragmentation pattern will affect data analysis methods such as pattern recognition and multivariate analysis. Also, changes in the fragmentation pattern will make it difficult to compare data between labs that use different ion sources. To address theses challenges, we carried out ToF-SIMS analysis of several adsorbed protein films using both monoatomic and cluster primary ion sources and then analyzed the differences in the fragmentation patterns with PCA.

In this study Cs^+, Au^+, Au_3^+, Bi^+, Bi_3^+, Bi_3^{++}, C_{60}^+, and C_{60}^{++} primary ion sources were used to generate mass spectra for four single-component proteins (albumin, fibrinogen, immunoglobulin G, and lysozyme) adsorbed onto mica. The goal of this analysis was to investigate how the differences between ion sources for a given protein compare to the differences between different proteins for a given ion source. The results of this study show how the combination of ToF-SIMS with PCA can be used to identify the influence of primary ion type on secondary ion fragmentation patterns.

2. Materials and Methods

2.1. Protein Adsorption for ToF-SIMS Analysis

Protein adsorption experiments were performed at 37°C for 2 hrs in CPBSz buffer (0.11M NaCl, 0.01M sodium citrate, 0.01M NaH2PO4, 0.02% NaN3, pH = 7.4) [37] onto freshly cleaved mica substrates (SPI Supplies, West Chester, PA) at a concentration of 100 μg/mL. Citrate is a chelating agent for the inhibition of protease activity, and azide is a phosphorylation inhibitor. After adsorption, the samples were first rinsed using dilution displacement to remove the protein solution. The samples were then taken out and rinsed in separate beakers for 1 minute each; twice in stirred CPBSz buffer to remove loosely bound protein and three times in stirred deionized water to remove buffer salts [4]. The samples were then dried under a stream of nitrogen and stored under nitrogen until analysis. Bovine serum albumin (BSA, A-2153), bovine serum fibrinogen (Fgn, F-8630)), bovine immunoglobulin G (IgG, I-5506), and chicken egg white lysozyme (Lys, L-6876) were purchased from Sigma (St. Louis, MO). All proteins were reconstituted into CPBSz buffer at a concentration of 1 mg/mL.

2.2. Atomic Force Microscopy (AFM)

Topography data of the proteins were acquired with Multimode IV atomic force microscope (Veeco Metrology, Santa Barbara, CA) using an NPS tip with 0.6 N/m force constant in contact mode. The thickness of the dried protein films were measured using a lithography-like method. First, an area of 500 nm × 500 nm was scratched into the films with a force setpoint of 4V to ensure that the protein film was removed and the substrate was not scratched, and then the force setpoint was decreased to 0V and the scan area was increased

to 2 μm × 2 μm to obtain an image of the crater. Three craters were formed and measured in various locations of the sample to calculate an average thickness for each sample.

2.3. Electron Spectroscopy for Chemical Analysis (ESCA)

Survey (0-1100 eV, analyzer pass energy = 150 eV) spectra were obtained using a Surface Science Instruments S-Probe spectrometer equipped with a monochromatized Al $K\alpha_{1,2}$ X-ray source (hv = 1486.6 eV) and a hemispherical electron energy analyzer. All the spectra were taken at a 55° photoelectron take-off angle (the photoelectron take-off angle is defined as the angle between the sample surface normal and the axis of the analyzer lens. Three spots on two replicates of each sample were analyzed. The composition data shown are averages of the values determined at all spots. Data analysis was performed using Service Physics ESCA 2000 A software (Bend, OR).

2.4. Time-of-Flight Secondary Ion Mass Spectrometry (ToF-SIMS)

Positive ion spectra were acquired using three ToF-SIMS instruments, each equipped with unique primary ion species and a pulsed flood gun for charge neutralization: PHI Model 7200 ToF-SIMS (Physical Electronics, Eden Prarie, MN) with a Cs^+ primary ion beam (8 keV); ION-TOF TOF.SIMS 5-100 (ION-TOF, Muenster Germany) with Au^+ and Au_3^+ primary ion beams (both 25 keV); and another ION-TOF 5-100 with Bi^+ (25 keV), Bi_3^+ (25 keV), Bi_3^{++} (50 keV), C_{60}^+ (10 keV) and C_{60}^{++} (20 keV) primary ion beams. Analysis areas were constrained to 150 μm × 150 μm, while maintaining a primary ion dose density of 10^{12} ions/cm^2 or below to ensure static SIMS conditions. The mass resolutions (m/Δm) for Cs^+ and liquid metal ion sources were typically above 6000, while those of C_{60}^+ and C_{60}^{++} were around 2500 and 4000, respectively. The spectra were calibrated to the CH_3^+, $C_2H_3^+$, $C_3H_5^+$, and $C_4H_7^+$ peaks before further analysis. Three spots on four replicates of each sample were analyzed.

2.5. Data Analysis

Two peaks sets were used for PCA processing of the ToF-SIMS data. One contained just amino acid fragments and the other contained all peaks from *m/z* 12 to 200. The peaks in each spectrum were normalized to the sum of the selected intensities to correct for variations in the total secondary ion yields between different spectra. The data were then mean-centered. Multivariate analysis was performed using PCA provided by a script written in-house for MATLAB (the MathWorks, Inc., Natick, MA), the theory of which is described in detail elsewhere [4, 7]. Briefly, PCA is a multivariate analysis method that determines the major directions of variation within a data set. To accomplish this, a data matrix is created where the rows (samples) contain data from individual spectra and the columns (variables) are measured areas from peaks within the spectra. PCA is then done using the singular value decomposition of the variance-covariance matrix of the normalized and mean-centered data set. Three new matrices are created, the scores, loadings, and residuals. The scores are a projection of the original samples onto the new principal component (PC) axes and show differences (if any) between the samples. The loadings are the direction cosines between the original variables and the new PC axes. The loadings show how the original variables relate to the differences seen between the samples on a given PC axis. The residuals are assumed to represent random noise. PCA scores and loadings plots are interpreted together using the following general guidelines. Samples with high scores on a given side of a PC axis correspond with variables with high loadings on the same side of the given PC axis. This means that, in general, samples with high scores on the positive the first PC (PC1) axis will show higher relative intensities for peaks with high loadings on the positive PC1 axis.

For this analysis, ToF-SIMS data where the intensity of the sodium ion peak was greater than 1% of the total intensity of the selected peaks were discarded due to matrix effects of

the sodium ion on the SIMS ionization process. Previous observations have shown that the inclusion of spectra with high sodium ion counts increased the within-group scatter of the data and decreased the ability to differentiate between the spectra of different proteins [5, 11].

3. Results and Discussion

The difference in the ToF-SIMS fragmentation pattern of proteins adsorbed onto mica surfaces was investigated as a function of primary ion species. This difference in the relative intensities of protein fragments were compared using two sets of variables; the amino acid peak list identified by Mantus et al. [2], and all peaks from *m/z* 12 – 200 with raw intensities above 1000 counts, including peaks from the mica substrate.

3.1. PCA Results of Individual Proteins using the Amino Acid Peak Set

For this dataset, four protein films were analyzed with eight primary ion beams, and PCA was performed using the amino acid peak list [2]. Scores and loadings plots for BSA and Fgn are shown in Figure 1. As seen in Figure 1, PC1 suggests that the greatest variation within the dataset is due to differences among primary ion species. There is a statistically significant separation between monatomic, tri-atomic, and polyatomic primary ions. The trend suggests that the variations in the relative intensities of the ejected secondary ions are significantly influenced by the differences in the collision cascade induced by the bombardment of monatomic, tri-atomic, and polyatomic ions. Molecular Dynamic (MD) simulations show that monatomic and polyatomic ions differ in their collision cascades [38-43]; they differ in primary ion range, crater dimension, and direction and extent of both energy transfer and atom displacement. Although discussion of secondary ion size variation as a function of primary ion species was not made in the above cited studies, it was inferred that different collision mechanisms would produce differences in secondary ion size. For the scores plot shown in Figure 1, the trend that separates primary ion species is similar for both BSA and fibrinogen, as well as for other proteins (for IgG and lysozyme results see Supporting Information). Also, small separations were seen for primary ions with different incident energies (singly and doubly charged Bi_3 with energies of 25 and 50 keV, respectively, as well as singly and doubly charged C_{60}, with energies of 10 and 20 keV, respectively). These observations support the MD simulations that cluster size of primary ion species influences collision cascades, which produce differences in the low mass (0-200 m/z) fragmentation pattern of the adsorbed proteins.

PC1 loadings plots were very similar for BSA, fibrinogen, and other proteins (IgG and lysozyme results shown in Supporting Information). Aside from small differences, they all had peaks at *m/z* 44, 70, 72, 84, 86, and 110 in the positive PC1 loadings, and peaks at *m/z* 18, 30, 43, 60, 61, 69, 71, 81, 82, and 87 in the negative PC1 loadings. This similarity among the four protein types is most likely due to the fact that these proteins are similar in amino acid composition, since they are composed of the same 20 amino acids. This illustrates the difficulty of trying to identify a single protein type within a multi-component mixture such as blood plasma. But as will be discussed later, these proteins do have small differences that can be identified using multivariate analysis [6, 7]. In the loadings plot, the intensities of the peaks mentioned above were shown to depend on the type of primary ion used. Table 1 lists the largest peaks in the loadings plot with their corresponding normalized intensity. Peak intensity analysis of the normalized data showed that peaks loading positively in Figure 1 decreased in intensity when the primary ion species was changed from monatomic to tri-atomic to polyatomic. Conversely, peaks loading negatively increased in intensity when the primary ion species was changed from monatomic to tri-atomic to polyatomic. For example, the positively loaded *m/z* 70 peak was the largest normalized peak in the spectra generated by monatomic primary ions (24% of the normalized intensity), but

its intensity decreased in the spectra generated by tri-atomic ions and further decreased for spectra generated by polyatomic ions (18%). The trend is reversed for the *m/z* 30 peak, which is negatively loaded. The normalized intensity of *m/z* 30 increased from about 12% of the normalized spectra generated by monatomic ions, to about 15% in the spectra generated by tri-atomic ions, and further increased to 20% in the spectra generated by polyatomic ions. Similar trends were seen for the rest of the peaks mentioned above, although the trends were not as pronounced as those observed for the *m/z* 30 or 70 peaks, since these were the two most dominant peaks in the normalized spectra. In general, cluster ions produced spectra with higher intensities of the lowest mass peaks, especially those below *m/z* 70.

Multivariate analysis, together with peak intensity analysis showed that there is a definite change in the adsorbed protein low mass fragmentation pattern when using different primary ions. These differences appear to be related to differences in the collision cascade caused by changes in the cluster size and kinetic energy of the primary ion. Since only the amino acid peak lists were used in the multivariate analysis, a general conclusion cannot be made here, but it appears that C_{60} primary ions may increase the fragmentation of adsorbed proteins.

3.2. PCA Results of All Proteins using the Amino Acid Peak Set

Figure 2 was constructed by combining the spectra of all proteins acquired using the eight different primary ion species. The scores cross-plot in this figure has PC1 on the x-axis and PC2 on the y-axis. As expected, PC1 shows that the greatest variation within the dataset is due to spectral differences caused by primary ions species, as indicated by separation of the data by primary ion type. PC2, the second greatest variation in the dataset, separates the data according to the amino acid composition of the proteins. This means that the differences in amino acid composition between proteins are smaller than differences in the relative intensity of fragments produced from different primary ion species. The trend in PC1 is very similar to the one seen earlier in Figure 1; the primary ions species are arranged in the order of increasing cluster size and kinetic energy with the same peaks in the loadings plot responsible for the separation. Again, the plot shows that larger clusters correspond with the emission of smaller secondary ion fragments.

PC2 separates the individual proteins in one order, regardless of the primary ion species used. The PC2 scores decrease in the order Lys, Fgn, IgG, and BSA. Even though the protein data acquired using $C_{60}^{+/++}$ are slightly offset towards the negative scores on the PC2 axis relative to other primary ion species, the protein order is still conserved. The PC2 loadings (Figure 2c) indicate that this ordering is due to differences in the amino acid compositions of the proteins. With Lys, for example, all of the primary ions have spectra where the intensity of the amino acid fragments at *m/z* 43 (a characteristic fragment of Arg), 44 (Ala), 70 (Asn), 73 (Arg), 86 (Ile/Leu), 100 (Arg), 130 (Trp), and 159 (Trp) are higher, which most likely reflects the greater proportion of these amino acids in Lys compared to the other proteins studied. BSA, which has the highest negative PC2 scores, should then have a lower concentration of the above mentioned amino acids. In fact, the comparison of compositions revealed that the proportion of these amino acids were greater in Lys. Arginine, alanine, asparagines, isoleucine, leucine, and tryptophan concentrations in Lys were approximately 8.5%, 9.3%, 10.9%, 4.7%, 6.2%, and 4.7% [44], while their concentrations in BSA were approximately 4.3%, 7.9%, 2.3%, 2.5%, 10.7%, and 0.5% [45]. Generally, amino acid composition differences among proteins were reflected in the PCA plots.

Although these differences in amino acid composition are very subtle, PCA is able to identify and differentiate the proteins [6, 7], assuming that spectral data was collected using the same primary ion source. Therefore caution should be used when comparing spectral data collected using two or more primary ion species, since differences in the fragmentation

pattern could overwhelm the variation in amino acid fragments. For example, a PCA model of BSA created with Cs^+ to determine the presence of BSA in blood serum using techniques such as SIMCA (soft independent modeling of class analogy) should only be applied to datasets obtained using Cs^+ [6, 7]. The difference in the relative intensity of secondary ion fragments sputtered by the different primary ions can overwhelm the variation in relative intensity of amino acid fragments between proteins, as was indicated by PC1 in Figure 2. This result suggests that the "characteristic" low mass amino acid fragmentation pattern depends on the type of primary ion used, especially for C_{60} ions. Although the PC2 loadings plot shows separation of proteins based on these characteristic fragments even for C_{60}, it should be noted that the PCA plots here were constructed using a very limited number of variables. The next section discusses the results when all the secondary ion peaks are used in PCA.

3.3. PCA Results of All Proteins using All Peaks from m/z 12-200

To assess the effects of secondary ion fragments other than characteristic amino acid fragments, PCA plots were constructed using all of the peaks in the range of *m/z* 12-200. For this study, the Au and Cs data were not included because they were unavailable.

Consistent with results from the previous section, the scores plot in Figure 3a again showed separation by primary ion type on PC1, and separation by protein composition on PC2. The loadings plot of PC1 in Figure 3b is similar to the previous PC1 loadings shown in Figure 2b. Even with using all of the secondary ion peaks, the spectra generated by the monatomic ions corresponded with higher intensity of the same amino acid fragments *m/z* 44 (Ala), 70 (Pro), 72 (Val), 84 (Lys), 86 (Ile/Leu), 110 (His), and 120 (Phe), while the spectra generated by the C_{60} ions corresponded with lower emission of these fragments. By using all peaks, the difference in fragmentation pattern became more apparent. Spectra acquired using Bi_1^+ and Bi_3^+ were similar and showed higher intensities of amino acid fragments listed above. In contrast the intensities of these same peaks were lower in spectra acquired using C_{60} ions. As mentioned previously, this suggests that amino acid fragmentation pattern changes depending on the primary ion species used to generate the spectra. Furthermore, peak intensity analysis showed that spectra generated with C_{60} primary ions corresponded with lower intensity of higher mass fragments in the m/z < region, indicating that the extent of fragmentation is most likely enhanced for higher order cluster ions. Studies of thin benzene films by Czerwinski and Postawa also showed that the main difference between the impacts of Ga and C_{60} primary ions were the extent of fragmentation of the organic molecule, where a six-fold increase in the intensity of fragmented benzene was observed with C_{60} primary ions [46, 47].

In PC2, the proteins were separated not by amino acid composition, but by the mica substrate (*m/z* 39 K^+) and a protein fragment (*m/z* 70 $C_4H_8N^+$). The arrangement of proteins on the PC2 scores plot is different from that seen in previous scores plots. In this scores plot, all of the primary ion species displayed the same ordering of the proteins; from positive to negative PC2 scores, it was BSA > Lys > IgG > Fgn. The ordering is independent of primary ion, and is based on of the thickness of the protein film. The solution concentration of 0.1 mg/mL used to deposit the protein films have been reported to give a packed monolayer [48, 49]. Although the nitrogen content measured by ESCA agreed with previously determined values [4, 6, 7], exposure of the sample to the atmosphere most likely results in denaturing of these proteins. Therefore, the thickness of the protein films could differ from the values expected from their dimensions in the native state. Also, the protein shapes are not spherical, so orientation of the absorbed protein molecules will affect the film thickness. Thus, protein film thicknesses were measured experimentally using an AFM tip scratch method rather than calculating the thickness from the known dimension of their native structures. The AFM measured thicknesses were 1.8 nm (BSA), 2.4 nm (Lys), 5.1 nm

(IgG) and 10.0 nm (Fgn), as shown in Table 2. Using ESCA, Wagner et al. have suggested that the natural log of the ratio of a protein overlayer signal to a substrate signal is proportional to the thickness of the protein layer [6]. This provides another method of validating the AFM data. Figure 4a shows the natural log of the ratio of the N_{1s} intensity (unique to the protein film) to the Al_{2s} intensity (unique to the mica substrate) plotted as a function of AFM thickness. As can be seen, there is a straight line correlation between the ESCA and AFM thickness measurements.

PC2 shows that there is a higher intensity of protein signal (*m/z* 70 $C_4H_8N^+$) for thicker films, and a higher substrate signal (*m/z* 30 K^+) for thinner films. Using this thickness data, it is now reasonable to assume that $C_4H_8N^+$ is a fragment that can be used to qualitatively measure the amount of protein on the surface ($C_4H_8N^+$ is common to all proteins under investigation). Also, it can be assumed that K^+ is a substrate signal that can be used to indirectly measure the amount of protein on mica substrates by looking at its signal attenuation since ToF-SIMS is a surface sensitive technique.

Similar to the protein-substrate ratio used for ESCA, the ratio of the key ToF-SIMS peak intensities in PC2 ($C_4H_8N^+$ to K^+) were plotted against film thickness to investigate whether these ToF-SIMS fragments can be used to determine the overlayer thickness (Figure 4b). It was found that the intensity ratio generally increased with thickness, with the increase being linear for Bi^+ and $Bi_3^{+/++}$ primary ions and exponential for $C_{60}^{+/++}$ primary ions (data from Bi_3^{++} and C_{60}^{++} primary ions are not shown since they overlapped with their respective singly charged counterparts). The linear trend of Bi^+ primary ion data indicates that this primary ion species generates surface sensitive spectra. An increase in film thickness leads to increased attenuation of the substrate signal. The C_{60}^+ primary ion generates lower values of the $C_4H_8N^+$ to K^+ ratio than the Bi^+ primary ion source for BSA, Lys and IgG. However, for the thickest protein film (Fgn) the $C_4H_8N^+$ to K^+ ratio generated by the Bi^+ and C_{60}^+ primary ions is similar. This suggests that for the thinner protein films C_{60} bombardment is more effective at sputtering off the protein film and exposing the substrate [50]. Since the thickness difference between the adsorbed BSA and Lys films can be distinguished in the spectra generated by Bi^+ primary ions, this suggests that for a “soft” overlayer (protein) on a “hard” substrate (mica) the spectra generated by Bi^+ primary ions are more surface sensitive than the spectra generated by C_{60}^+ primary ions.. Spectra generated by Bi_3^+ primary ions are observed to be the least surface sensitive as all protein films exhibit a large intensity of the substrate peak (K^+).

4. Conclusion

The PCA comparison of ToF-SIMS data showed that differences in the protein fragmentation pattern caused by the primary ions were greater than differences in protein composition. This is likely because the different fragmentation pathways created by the collision cascade of the different primary ions overwhelmed the variation in relative intensity of amino acid fragments between proteins. In particular, the increased extent of fragmentation in the low mass region ($m/z < 200$) observed in spectra generated by C_{60} primary ions results in more intense low *m/z* peaks. This study showed that comparison of data obtained by one primary ion species with that obtained by another primary ion species should be done with caution. The spectra generated by Cs^+, Au^+ and Bi^+ primary ions were similar, but the spectra generated by monatomic, tri-atomic and polyatomic primary ion ions varied significantly. However, for the spectra generated a given primary ion beam, the separation of the different proteins followed similar trends. Therefore, a PCA model of a protein created with a given ion source should be applied to datasets obtained using the same ion source.

This study also demonstrated that the choice of variables used in PCA can affect the type of information extracted from the dataset. When only amino acid peaks were used, PC2 was able to identify the relationship of proteins by their amino acid composition. When all peaks from *m/z* 12-200 were used, the separation of the proteins was based on a ratio of $C_4H_8N^+$ to K^+ peak intensities that was shown to correlate to the thickness of the protein films. Interestingly, the $C_4H_8N^+/K^+$ ratio from Bi_1^+ primary ions varied linearly with protein thickness, suggesting that this ion source may produce the most surface sensitive spectra.

Supplementary Material

Refer to Web version on PubMed Central for supplementary material.

Acknowledgments

The authors gratefully acknowledge support of grant EB-002027 from the NIH to NESAC/Bio for these studies.

References

1. Ferrari S, Ratner BD. ToF-SIMS quantification of albumin adsorbed on plasma-deposited fluoropolymers by partial least-squares regression. Surface and Interface Analysis. 2000; 29(12): 837–844.
2. Mantus DS, Ratner BD, Carlson BA, Moulder JF. Static secondary ion mass spectrometry of adsorbed proteins. Analytical Chemistry. 1993; 65(10):1431–1438. [PubMed: 8517550]
3. Tidwell CD, Castner DG, Golledge SL, Ratner BD, Meyer K, Hagenhoff B, Benninghoven A. Static time-of-flight secondary ion mass spectrometry and x-ray photoelectron spectroscopy characterization of adsorbed albumin and fibronectin films. Surface and Interface Analysis. 2001; 31(8):724–733.
4. Wagner MS, Castner DG. Characterization of Adsorbed Protein Films by Time-of-Flight Secondary Ion Mass Spectrometry with Principal Component Analysis. Langmuir. 2001; 17(15):4649–4660.
5. Wagner MS, Tyler BJ, Castner DG. Interpretation of Static Time-of-Flight Secondary Ion Mass Spectra of Adsorbed Protein Films by Multivariate Pattern Recognition. Analytical Chemistry. 2002; 74(8):1824–1835. [PubMed: 11985314]
6. Wagner MS, Horbett TA, Castner DG. Characterization of the Structure of Binary and Ternary Adsorbed Protein Films Using Electron Spectroscopy for Chemical Analysis, Time-of-Flight Secondary Ion Mass Spectrometry, and Radiolabeling. Langmuir. 2003; 19(5):1708–1715.
7. Wagner MS, Horbett TA, Castner DG. Characterizing multicomponent adsorbed protein films using electron spectroscopy for chemical analysis, time-of-flight secondary ion mass spectrometry, and radiolabeling: capabilities and limitations. Biomaterials. 2003; 24(11):1897–1908. [PubMed: 12615480]
8. Hillenkamp F, Karas M, Beavis RC, Chait BT. Matrix-assisted laser desorption/ionization mass spectrometry of biopolymers. Anal. Chem. 1991; 63(24):1193–1203. [PubMed: 1897719]
9. Menzel C, Berkenkamp S, Hillenkamp F. Infrared matrix-assisted laser desorption/ionization mass spectrometry with a transversely excited atmospheric pressure carbon dioxide laser at 10.6 μm wavelength with static and delayed ion extraction. Rapid Communications in Mass Spectrometry. 1999; 13(1):26–32.
10. Belu AM, Graham DJ, Castner DG. Time-of-flight secondary ion mass spectrometry: techniques and applications for the characterization of biomaterial surfaces. Biomaterials. 2003; 24(21):3635–3653. [PubMed: 12818535]
11. Lhoest JB, Wagner MS, Tidwell CD, Castner DG. Characterization of adsorbed protein films by time of flight secondary ion mass spectrometry. Journal of Biomedical Materials Research. 2001; 57(3):432–440. [PubMed: 11523038]
12. Michel R, Castner DG. Advances in time-of-flight secondary ion mass spectrometry analysis of protein films. Surface and Interface Analysis. 2006; 38(11):1386–1392.

13. Michel R, Pasche S, Textor M, Castner DG. Influence of PEG architecture on protein adsorption and conformation. Langmuir. 2005; 21(26):12327–12332. [PubMed: 16343010]
14. Wagner MS, Castner DG. Characterization of adsorbed protein films using time-of-flight-secondary ion mass spectrometry and multivariate analysis. Applied Surface Science. 2003; 203:698–703.
15. Xia N, Castner DG. Preserving the structure of adsorbed protein films for time-of-flight secondary ion mass spectrometry analysis. Journal of Biomedical Materials Research Part A. 2003; 67A(1): 179–190. [PubMed: 14517875]
16. Xia N, May CJ, McArthur SL, Castner DG. Time-of-flight secondary ion mass spectrometry analysis of conformational changes in adsorbed protein films. Langmuir. 2002; 18(10):4090–4097.
17. Bruuning C, Hellweg S, Dambach S, Lipinsky D, Arlinghaus HF. Improving the interpretation of ToF-SIMS measurements on adsorbed proteins using PCA. Surface and Interface Analysis. 2006; 38(4):191–193.
18. Jones EA, Fletcher JS, Thompson CE, Jackson DA, Lockyer NP, Vickerman JC. ToF-SIMS analysis of bio-systems: Are polyatomic primary ions the solution? Applied Surface Science. 2006; 252(19):6844–6854.
19. Kim YP, Hong MY, Kim J, Oh E, Shon HK, Moon DW, Kim HS, Lee TG. Quantitative analysis of surface-immobilized protein by TOF-SIMS: Effects of protein orientation and trehalose additive. Analytical Chemistry. 2007; 79(4):1377–1385. [PubMed: 17297937]
20. Sanni OD, Wagner MS, Briggs D, Castner DG, Vickerman JC. Classification of adsorbed protein static ToF-SIMS spectra by principal component analysis and neural networks. Surface and Interface Analysis. 2002; 33(9):715–728.
21. Wagner MS, Graham DJ, Ratner BD, Castner DG. Maximizing information obtained from secondary ion mass spectra of organic thin films using multivariate analysis. Surface Science. 2004; 570(1-2):78–97.
22. Henry M, Dupont-Gillain C, Bertrand P. Conformation change of albumin adsorbed on polycarbonate membranes as revealed by ToF-SIMS. Langmuir. 2003; 19(15):6271–6276.
23. Appelhans AD, Delmore JE. Comparison of polyatomic and atomic primary beams for secondary ion mass-spectrometry of organics. Analytical Chemistry. 1989; 61(10):1087–1093.
24. Benguerba M, Brunelle A, Dellanegra S, Depauw J, Joret H, Lebeyec Y, Blain MG, Schweikert EA, Benassayag G, Sudraud P. Impact of slow gold clusters on various solids - nonlinear effects in secondary ion emission. Nuclear Instruments & Methods in Physics Research Section B-Beam Interactions with Materials and Atoms. 1991; 62(1):8–22.
25. Touboul D, Kollmer F, Niehuis E, Brunelle A, Laprevote O. Improvement of biological time-of-flight-secondary ion mass spectrometry imaging with a bismuth cluster ion source. Journal of the American Society for Mass Spectrometry. 2005; 16(10):1608–1618. [PubMed: 16112869]
26. Postawa Z, Czerwinski B, Szewczyk M, Smiley EJ, Winograd N, Garrison BJ. Enhancement of sputtering yields due to C-60 versus Ga bombardment of Ag{111} as explored by molecular dynamics simulations. Analytical Chemistry. 2003; 75(17):4402–4407. [PubMed: 14632043]
27. Wong SCC, Hill R, Blenkinsopp P, Lockyer NP, Weibel DE, Vickerman JC. Development of a C-60(+) ion gun for static SIMS and chemical imaging. Applied Surface Science. 2003; 203:219–222.
28. Benninghoven A, Hagenhoff B, Niehuis E. Surface MS - Probing real-world samples. Analytical Chemistry. 1993; 65(14):A630–A640.
29. Wu KJ, Odom RW. Matrix-enhanced secondary ion mass spectrometry: a method for molecular analysis of solid surfaces. Anal. Chem. 1996; 68(5):873–882. [PubMed: 21619183]
30. McArthur SL, Vendettuoli MC, Ratner BD, Castner DG. Methods for Generating Protein Molecular Ions in ToF-SIMS. Langmuir. 2004; 20(9):3704–3709. [PubMed: 15875403]
31. Adriaensen L, Vangaever F, Gijbels R. Metal-assisted secondary ion mass spectrometry: Influence of Ag and Au deposition on molecular ion yields. Analytical Chemistry. 2004; 76(22):6777–6785. [PubMed: 15538803]
32. Nygren H, Eriksson C, Malmberg P, Sahlin H, Carlsson L, Lausmaa J, Sjovall P. A cell preparation method allowing subcellular localization of cholesterol and phosphocholine with imaging TOF-SIMS. Colloids and Surfaces B-Biointerfaces. 2003; 30(1-2):87–92.

33. Delcorte A. Matrix-enhanced secondary ion mass spectrometry: The Alchemist's solution? Applied Surface Science. 2006; 252(19):6582–6587.
34. Lockyer NP, Vickerman JC. Single photon and femtosecond multiphoton ionisation of the dipeptide valyl-valine. International Journal of Mass Spectrometry. 2000; 197(1-3):197–209.
35. Weibel D, Wong S, Lockyer N, Blenkinsopp P, Hill R, Vickerman JC. A C-60 primary ion beam system for time of flight secondary ion mass spectrometry: Its development and secondary ion yield characteristics. Analytical Chemistry. 2003; 75(7):1754–1764. [PubMed: 12705613]
36. Brunelle A, Touboul D, Laprevote O. Biological tissue imaging with time-of-flight secondary ion mass spectrometry and cluster ion sources. Journal of Mass Spectrometry. 2005; 40(8):985–999. [PubMed: 16106340]
37. Horbett, TA. In Techniques of Biocompatibility Testing. Williams, DF., editor. CRC Press; Boca Raton, FL: 1968. p. 183-215.
38. Aoki T, Seki T, Matsuo J, Insepov Z, Yamada I. Molecular dynamics simulation of a carbon cluster ion impacting on a carbon surface. Materials Chemistry and Physics. 1998; 54(1-3):139–142.
39. Biersack JP, Haggmark LG. A Monte Carlo computer program for the transport of energetic ions in amorphous targets. Nuclear Instruments and Methods. 1980; 174(1-2):257–269.
40. Garrison BJ, Postawa Z. Computational view of surface based organic mass spectrometry. Mass Spectrometry Reviews. 2008; 27(4):289–315. [PubMed: 18421766]
41. Postawa Z, Czerwinski B, Szewczyk M, Smiley EJ, Winograd N, Garrison BJ. Enhancement of sputtering yields due to C-60 versus Ga bombardment of Ag{111} as explored by molecular dynamics simulations. Analytical Chemistry. 2003; 75(17):4402–4407. [PubMed: 14632043]
42. Russo MF, Garrison BJ. Mesoscale energy deposition footprint model for kiloelectronvolt cluster bombardment of solids. Analytical Chemistry. 2006; 78(20):7206–7210. [PubMed: 17037922]
43. Russo MF, Wojciechowski IA, Garrison BJ. Sputtering of amorphous ice induced by C-60 and Au-3 clusters. Applied Surface Science. 2006; 252(19):6423–6425.
44. Canfield RE. The Amino Acid Sequence of Egg White Lysozyme. Journal of Biological Chemistry. 1963; 238(8):2698–2707. [PubMed: 14063294]
45. Hirayama K, Akashi S, Furuya M, Fukuhara K.-i. Rapid confirmation and revision of the primary structure of bovine serum albumin by ESIMS and frit-FAB LC/MS. Biochemical and Biophysical Research Communications. 1990; 173(2):639–646. [PubMed: 2260975]
46. Postawa Z, Czerwinski B, Winograd N, Garrison BJ. Microscopic insights into the sputtering of thin organic films on Ag{111} induced by C-60 and Ga bombardment. Journal of Physical Chemistry B. 2005; 109(24):11973–11979.
47. Czerwinski B, Delcorte A, Garrison BJ, Samson R, Winograd N, Postawa Z. Sputtering of thin benzene and polystyrene overlayers by keV Ga and C60 bombardment. Applied Surface Science. 2006; 252(19):6419–6422.
48. Horbett TA. Principles underlying the role of adsorbed plasma proteins in blood interactions with foreign materials. Cardiovascular Pathology. 1993; 2(3):137–148.
49. Wahlgren M, Arnebrant T. Protein adsorption to solid surfaces. Trends in Biotechnology. 1991; 9(1):201–208. [PubMed: 1367245]
50. Postawa Z, Czerwinski B, Winograd N, Garrison B. Microscopic insights into the sputtering of thin organic films on Ag{1 1 1} induced by C60 and Ga bombardment. Journal of Physical Chemistry B. 2005; 109:11973–11979.

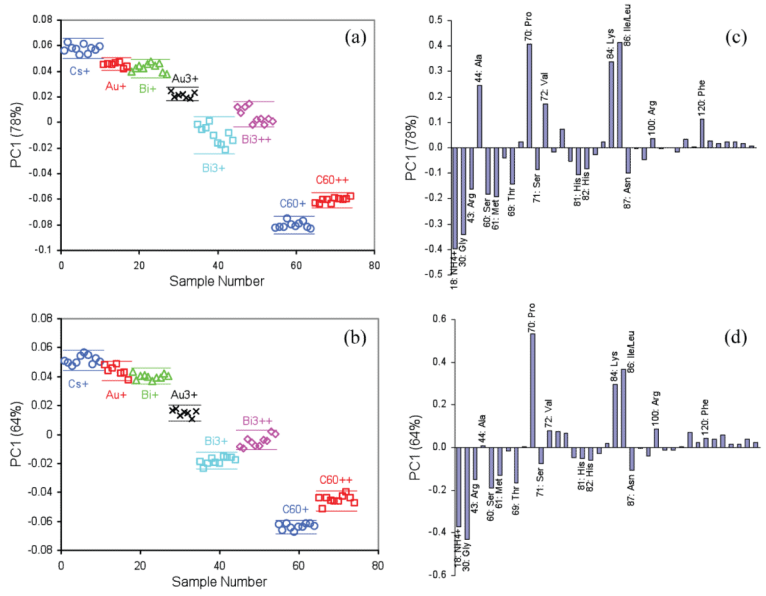

Figure 1.

PCA scores plots from ToF-SIMS analysis of (a) BSA and (b) Fgn adsorbed onto mica surfaces. The corresponding loadings plots for adsorbed BSA and Fgn are shown in (c) and (d), respectively. In the scores plot, the horizontal dotted lines represent the 95% confidence limits. The loadings plot shows the peaks in increasing mass, with the major peaks labeled. These loadings show which peaks are most responsible for the differences observed in the scores plots.

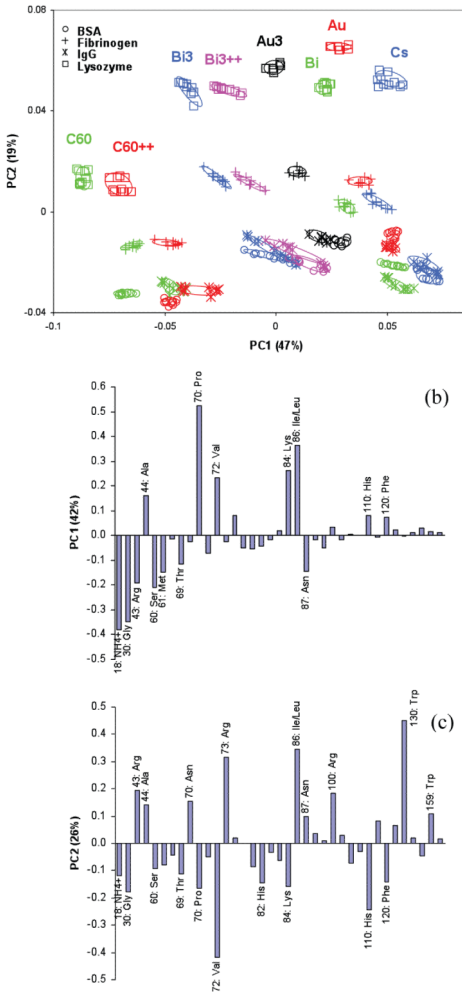

Figure 2.

PCA scores plot of (a) PC 1 vs. PC 2, and loadings plots of (b) PC1 and (c) PC2 for BSA, Fgn, Lys and I.gG adsorbed onto mica surfaces and analyzed with eight different primary ion beams. The ellipses represent the 95% confidence limits. The type of primary ion beams is color-coded and the type of adsorbed protein is identified by different symbols.

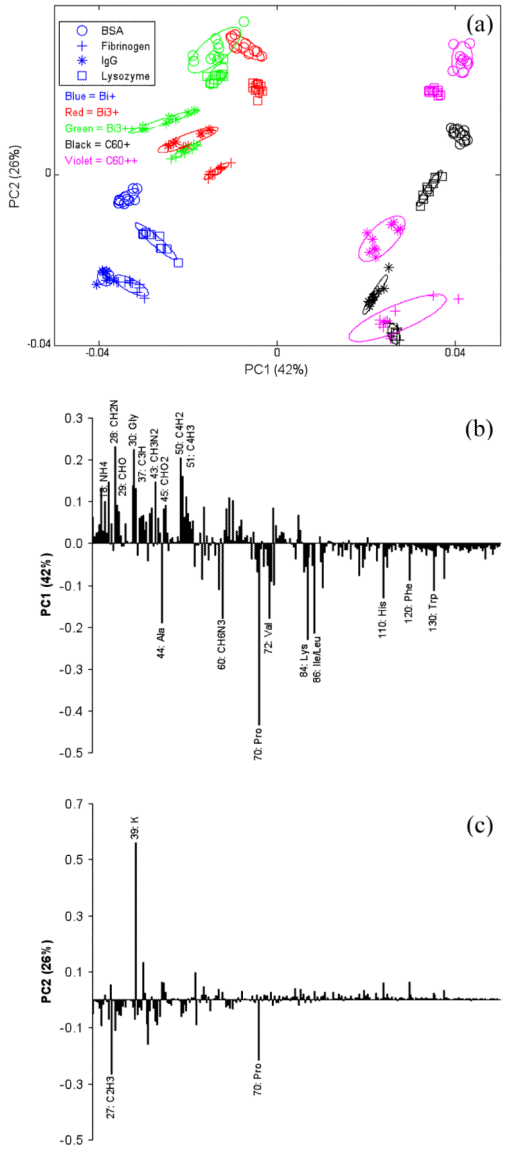

Figure 3.

(a) PCA scores plot of the four proteins adsorbed onto a mica surface and analyzed with five different primary ion beams. The corresponding loadings plots for (b) PC1 and (c) PC2 are shown with the major peaks labeled. The PCA dataset uses all peaks from *m/z* 12-200 to construct these plots.

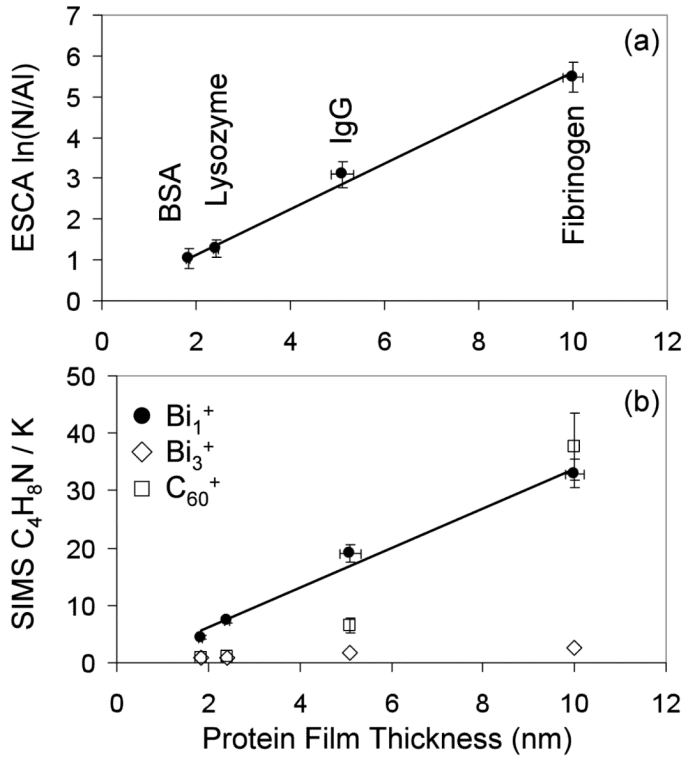

Figure 4.

(a) A comparison of the ESCA ratio and AFM film thickness. (b) A comparison of the ToF-SIMS ratio and AFM film thickness. The ESCA ratio is calculated by taking the logarithm of the quotient of N_{1s} and Al_{2s} signals, and the ToF-SIMS ratio is calculated by dividing $C_4H_8N^+$ peak intensity by the K^+ peak intensity. The error bars represent 95% confidence intervals, with the errors of AFM measurements shown only for Bi^+ in (b) for clarity.

Table 1

Summary of the six highest amino acid peaks emitted using the eight different primary ion sources for analyzying adsorbed BSA and Fgn. Values in parentheses are percent intensities normalized to the sum of selected peaks, which are *m/z* 18, 30, 43, 44, 69, 70, 72, 84, and 86. The peaks with the highest positive (m/z = 70) and negative (m/z = 30) PC1 loadings are highlighted in red.

Protein	Ion Source	Mass Number (% Normalized Intensity)					
BSA							
	Cs^+	70 (24)	44 (15)	84 (15)	86 (13)	72 (12)	**30** (11)
	Au^+	70 (21)	86 (16)	44 (14)	84 (13)	72 (12)	**30** (10)
	Bi^+	70 (24)	44 (15)	84 (14)	**30** (13)	86 (12)	72 (10)
	Au_3^+	70 (19)	44 (15)	86 (14)	**30** (13)	84 (12)	72 (11)
	Bi_3^+	70 (18)	**30** (17)	44 (15)	84 (12)	86 (11)	72 (10)
	Bi_3^{++}	70 (20)	**30** (16)	44 (16)	84 (12)	86 (10)	72 (9)
	C_{60}^+	**30** (20)	70 (16)	18 (14)	44 (11)	69 (9)	72 (8)
	C_{60}^{++}	**30** (20)	70 (19)	44 (13)	18 (11)	84 (8)	72 (7)
Fibrinogen							
	Cs^+	70 (31)	84 (16)	**30** (15)	44 (14)	86 (13)	72 (8)
	Au^+	70 (28)	86 (14)	**30** (14)	44 (13)	84 (12)	72 (9)
	Bi^+	70 (32)	**30** (16)	84 (14)	44 (12)	86 (11)	43 (8)
	Au_3^+	70 (24)	**30** (16)	44 (15)	86 (12)	84 (11)	43 (9)
	Bi_3^+	70 (20)	**30** (19)	44 (13)	84 (11)	86 (10)	43 (9)
	Bi_3^{++}	70 (23)	**30** (19)	44 (13)	84 (12)	86 (11)	43 (9)
	C_{60}^+	**30** (23)	70 (19)	44 (13)	18 (12)	69 (9)	43 (8)
	C_{60}^{++}	**30** (22)	70 (21)	44 (13)	18 (11)	43 (9)	69 (8)

Table 2

Thickness of adsorbed protein films on mica measured using a soft-lithography-like method with AFM. Three measurements were taken to calculate the average.

	Thickness (nm)
BSA	1.8 ± 0.1
Lysozyme	2.4 ± 0.1
IgG	5.1 ± 0.2
Fibrinogen	10.0 ± 0.3